Supplementary Material for

Multiple equilibrium states of a curved-sided hexagram: Part II—Transitions between states

Lu Lu[a], Jize Dai[a], Sophie Leanza[a], John W. Hutchinson[b], Ruike Renee Zhao[a,*]

[a] Department of Mechanical Engineering, Stanford University, Stanford, CA 94305, USA
[b] School of Engineering and Applied Sciences, Harvard University, Cambridge, MA 02138, USA

1. Fabrication of the curved-sided hexagram rings

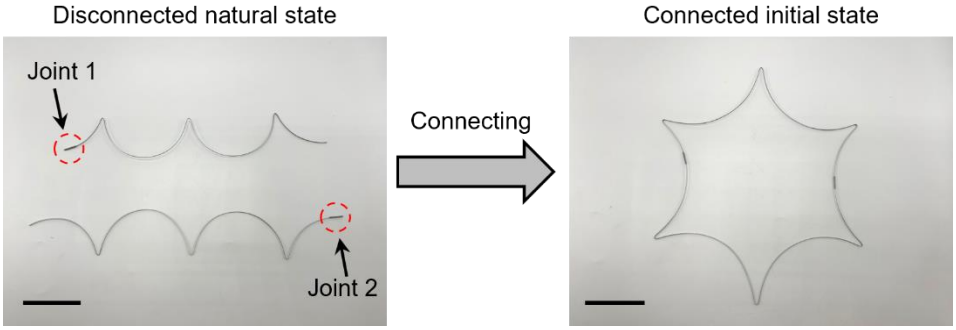

Fig. S1. Fabrication process of the star hexagram by connecting two long stainless-steel rods. Scale bars: 8cm.

The curved-sided hexagram rings presented in this work are fabricated by manually reshaping stainless-steel rods. During fabrication, small "corners" are introduced by applying plastic deformations to reshape the rod. When the corner size is relatively small, such as the 1 mm corner radius used in the current work, it has negligible effects on the stability and the transition behavior of the rings, which has been demonstrated in Figs. 3 and 6 in Part I. The four basic equilibrium states (i.e., the star hexagram, the daisy hexagram, the 3-loop line, and the 3-loop 8) shown in Fig. 1 in the main text all have the same edge length, L = 200 mm, and are fabricated using two 600 mm long stainless-steel rods with rectangular cross-section of height h = 2 mm and thickness t = 0.5 mm. Fig. S1 shows the fabrication process of the star hexagram as an example. First, we reshape the two long rods into multiple curved-sided segments by applying plastic deformations. Each long rod has three corners. Then, we connect the two rods using two joints to obtain the star hexagram. Note that the natural curvature of each segment can also be manually controlled by applying plastic deformation. The 6-circle hexagram rings shown in Fig. 4 in the main text are fabricated using the same method, except that six 600 mm stainless-steel rods were

used (each with only one corner) in order to achieve the desired natural curvature. In particular, the two 6-circle hexagram rings both can be deployed to an unstable star hexagram state with edge length L=600mm.

2. Transition behavior of the daisy hexagram

Transition behavior of the daisy hexagram with different natural curvatures under corner bend is presented in Fig. S2. The daisy hexagram has an edge radius of $3L/4\pi$ in the initial state, corresponding to a dimensionless initial curvature $L\kappa_0/2\pi = 2/3$. From Fig. S2, one can find that the daisy hexagram can transition to different states by rationally choosing its natural curvature. Specifically, the daisy hexagram with a dimensionless natural curvature, $L\kappa_n/2\pi$, in the range (0.32, 0.69), undergoes an inversion and transforms into the star hexagram. However, in the range (0.70, 1.09), it folds into the 3-loop "8" configuration. Also, it is seen that when the dimensionless natural curvature is smaller than 0.32, or larger than 1.09, the daisy hexagram is no longer stable in the initial state. Therefore, the lower and upper stability limits for the dimensionless natural curvature of the daisy hexagram is 0.32 and 1.09, which is in excellent agreement with the theoretical predictions in Part I for the case of h/t=4 and ν=1/3.

Transition behavior of the daisy hexagram with different natural curvatures within the stability range (0.32, 1.09), under edge bend, is shown in Fig. S3. It can be observed that when the dimensionless natural curvature, $L\kappa_n/2\pi$, is within the range (0.32, 0.62), the daisy hexagram inverts into the star hexagram. By contrast, when the dimensionless natural curvature falls in the range (0.63, 1.09), the daisy hexagram folds into the 3-loop "8" configuration. Compared with the results of corner bend, we can find that there is a small dimensionless natural curvature range (0.63, 0.69), including the dimensionless natural curvature of the stress-free daisy hexagram ($L\kappa_n/2\pi$=2/3), within which the daisy hexagram transitions to the star hexagram under corner bend, while transitions to the 3-loop "8" under edge bend. Therefore, transition behavior of the daisy hexagram depends not only on the natural curvature but also on the loading positions of the external stimuli.

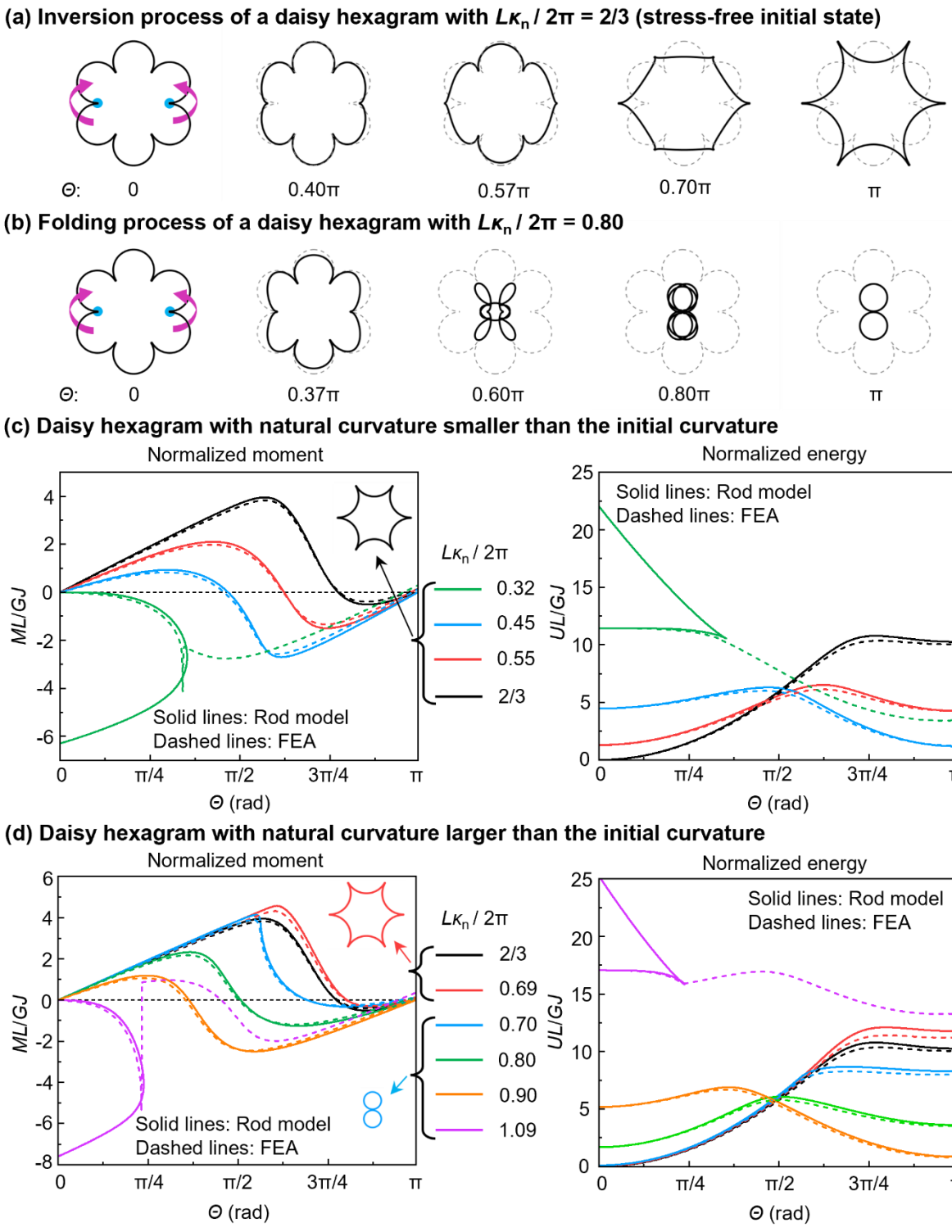

Fig. S2. Transition behavior of daisy hexagrams with different natural curvatures under corner bend. (a) Inversion process (top view) of a daisy hexagram with a dimensionless natural curvature $L\kappa_n/2\pi = 2/3$, which has a stress-free initial state. (b) Folding process (top view) of a daisy hexagram with a dimensionless natural curvature $L\kappa_n/2\pi = 0.80$. The blue dots denote the loading positions. (c) Normalized moment and energy versus bending angle of daisy hexagrams with natural curvatures smaller than the initial curvature.

(d) Normalized moment and energy versus bending angle of daisy hexagrams with natural curvatures larger than the initial curvature. The daisy hexagram with dimensionless natural curvature in the range (0.32, 0.69) inverts into the star hexagram, and in the range (0.70, 1.09) folds into the 3-loop "8", as indicated by the insets.

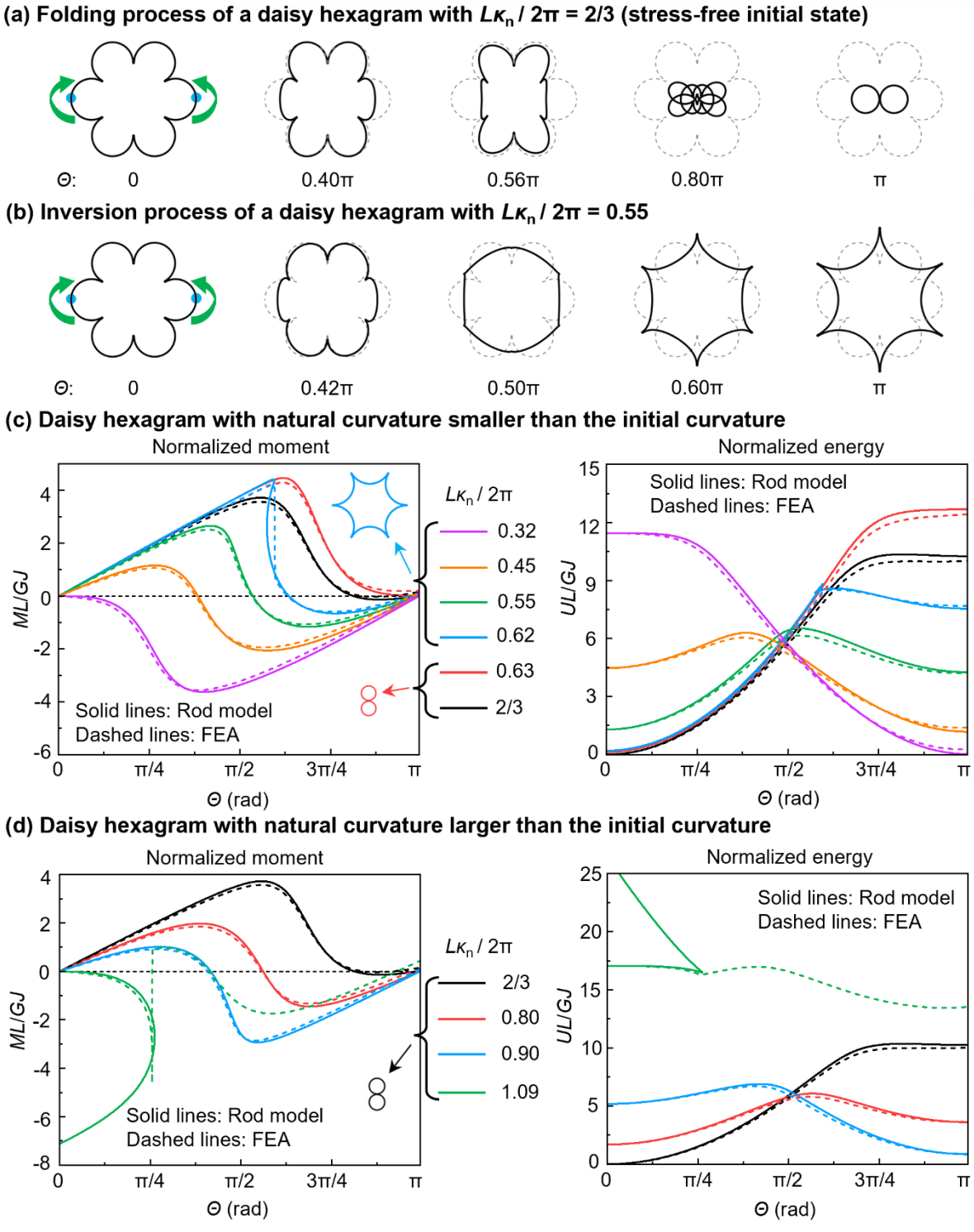

Fig. S3. Transition behavior of daisy hexagrams with different natural curvatures under edge bend. (a) Folding process (top view) of a star hexagram with a dimensionless natural curvature $L\kappa_n/2\pi = 2/3$, which has a stress-free initial state. (b) Inversion process (top view) of a star hexagram with a dimensionless natural curvature $L\kappa_n/2\pi = 0.55$. The blue dots denote the loading positions. (c) Normalized moment and energy versus bending angle of daisy hexagrams with natural curvatures smaller than the initial curvature. (d) Normalized moment and energy versus bending angle of daisy hexagrams with natural curvatures larger than the initial curvature. The daisy hexagram with dimensionless natural curvature in the range (0.32, 0.62) inverts into the star hexagram, and in the range (0.63, 1.09) folds into the 3-loop "8", as indicated by the insets.

3. Transition behavior of the 3-loop line and the 3-loop "8"

For a multiloop ring, there are multiple ways to trigger its state transition. The simplest way is to grab all layers together and then bend them at a pair of corners or edges. Using this method, the 3-loop line could invert into the 3-loop "8" and vice versa. Alternatively, one can bend a multiloop ring by holding a single layer at one corner (or edge) and grabbing another single layer at the opposite corner (or edge). By selecting appropriate layers on two sides of the ring, the 3-loop line and 3-loop "8" could unfold into the star hexagram and the daisy hexagram, respectively. It should be stated that different loading methods may produce different critical natural curvatures beyond which the multiloop ring becomes unstable. For the 3-loop line and the 3-loop "8", we find that the critical natural curvature obtained by bending the rings in different layers could reproduce the stability limits theoretically predicted by Part I. However, when bending the three layers together, much wider stability ranges than those in Part I are obtained.

In Part II, we discuss the transition behavior of the 3-loop line and 3-loop "8" within the stability range determined by bending in different layers. The transition behavior of the 3-loop line and the 3-loop "8" triggered by bending three layers together and by bending in different layers are both presented. Note that the results presented in Fig. 7 in the main text are produced by bending the three layers of the 3-loop line and 3-loop 8 together, because they can transform into each other such that the transitions between the four equilibrium states can be achieved.

3.1. Bending three layers together

Transition behavior of the 3-loop line with different natural curvatures within the stability range $(-0.73, 0.73)$, triggered by bending three layers together at a pair of corners or edges (referred to as corner bend or edge bend in the main text), is shown in Figs. S4 and S5, respectively. It is found that when bending the three layers together, the 3-loop line always transitions to a 3-

loop “8” state, regardless of the bending locations. However, the 3-loop line with zero or positive natural curvature inverts into a 3-loop “8” configuration with curved edges contacting in the middle, while the 3-loop line with negative natural curvature inverts into a 3-loop “8” configuration without edge contact in the middle.

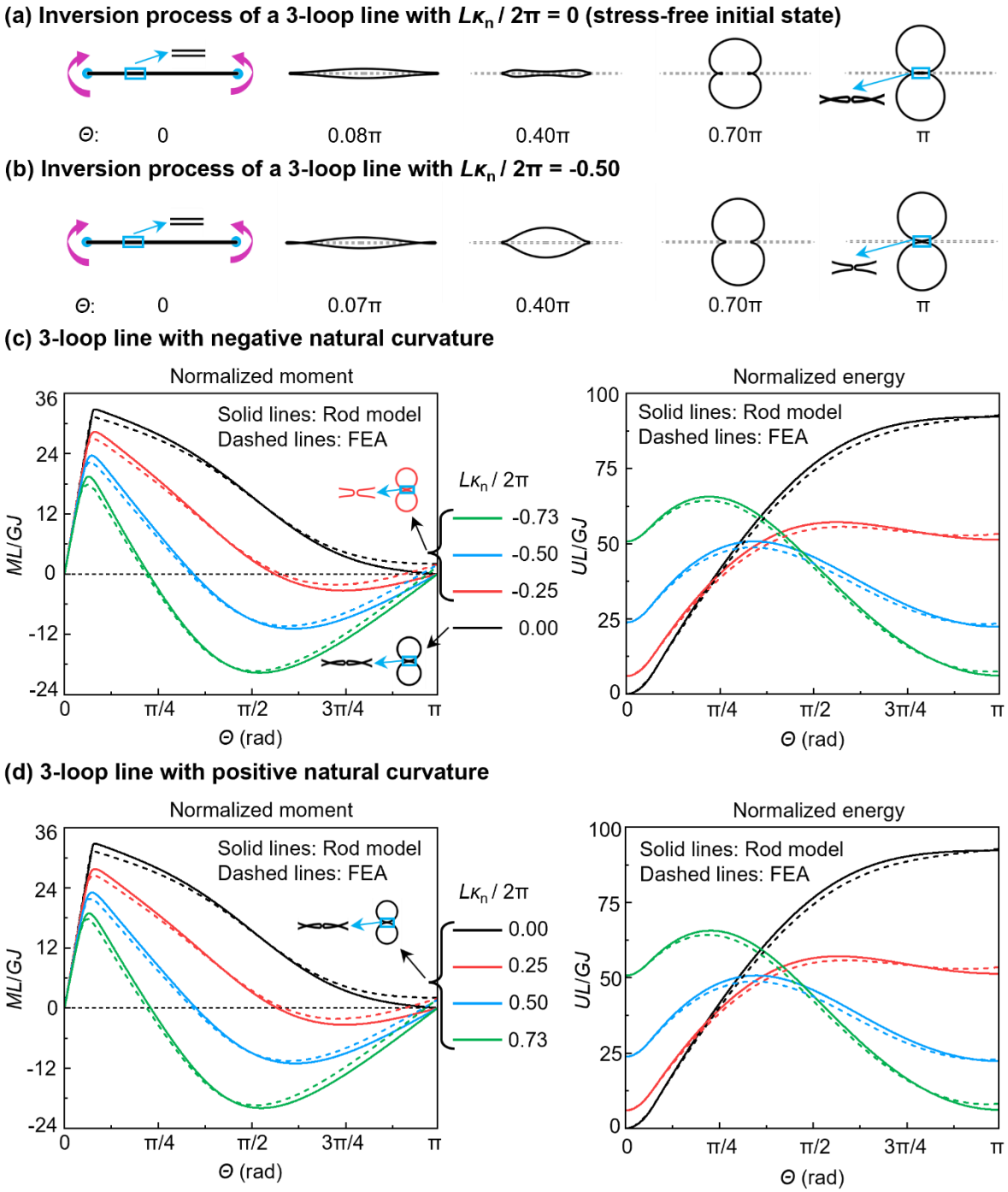

Fig. S4. Transition behavior of 3-loop lines with different natural curvatures under corner bend. (a) Inversion process (top view) of a 3-loop line with a dimensionless natural curvature $L\kappa_n/2\pi = 0$, which has a stress-free initial state. (b) Inversion process (top view) of a 3-loop line with a dimensionless natural curvature $L\kappa_n/2\pi = -0.5$. The blue dots denote the loading positions. (c) Normalized moment and energy versus bending angle of 3-loop lines with negative natural curvatures. (d) Normalized moment and energy versus bending angle of 3-loop lines with positive natural curvatures. The 3-loop line with dimensionless natural curvature in the range (−0.73, 0) inverts into a 3-loop "8" configuration without edge contact in the middle, and in the range (0, 0.73) inverts into a 3-loop "8" with edge contact in the middle, as indicated by the insets.

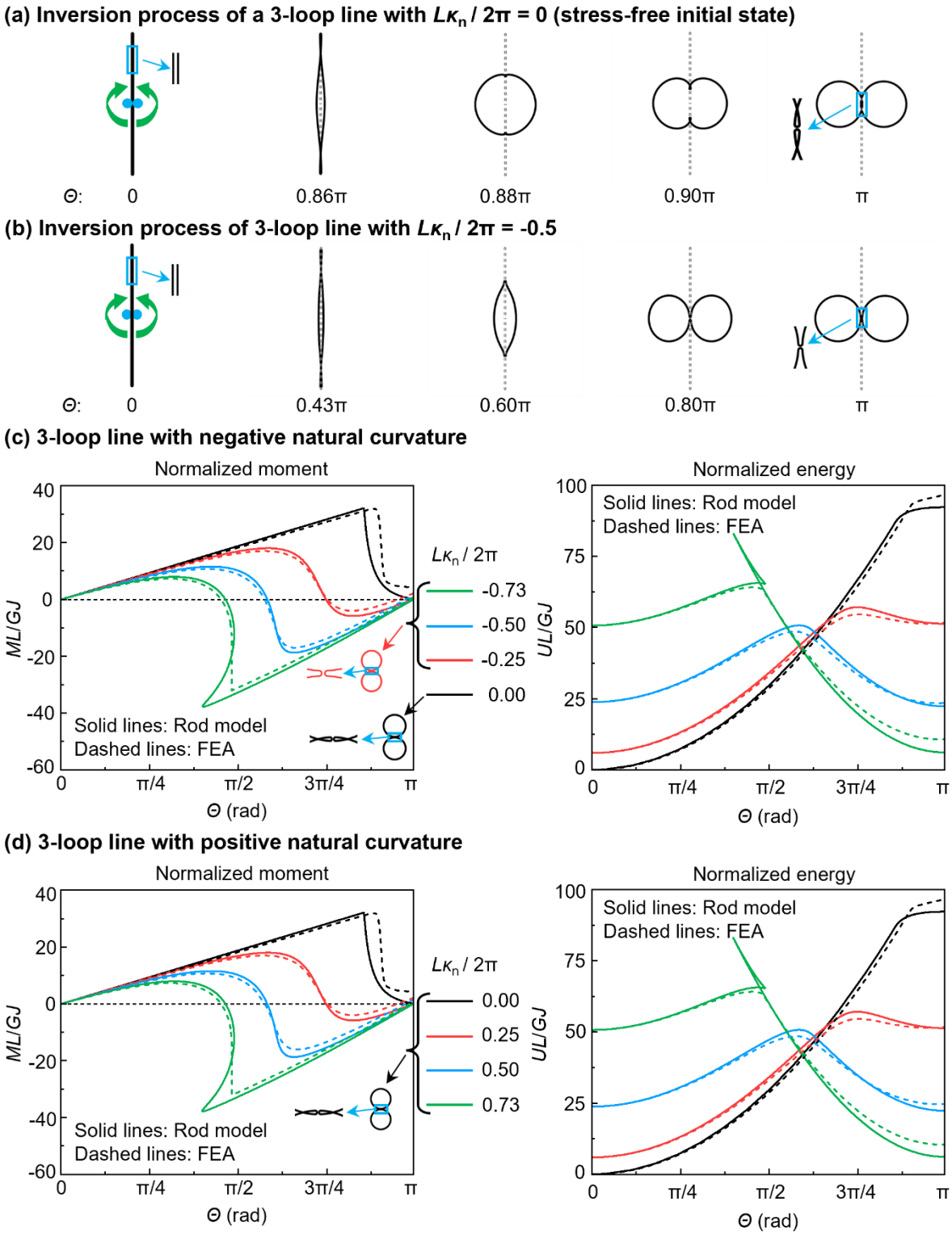

Fig. S5. Transition behavior of 3-loop lines with different natural curvatures under edge bend. (a) Inversion process (top view) of a 3-loop line with a dimensionless natural curvature $L\kappa_n/2\pi = 0$, which has a stress-free initial state. (b) Inversion process (top view) of a 3-loop line with a dimensionless natural curvature $L\kappa_n/2\pi = -0.5$. The blue dots denote the loading positions. (c) Normalized moment and energy versus bending angle of 3-loop lines with negative natural curvatures. (d) Normalized moment and energy versus

bending angle of 3-loop lines with positive natural curvatures. The 3-loop line with dimensionless natural curvature in the range (−0.73, 0) inverts into a 3-loop "8" configuration without edge contact in the middle, and in the range (0, 0.73) inverts into a 3-loop "8" with edge contact in the middle, as indicated by the insets.

Transition behavior of the 3-loop "8" with different natural curvatures within the stability range (0.64, 1.38), triggered by bending three layers together at a pair of corners (referred to as corner bend in the main text), is presented in Fig. S6. Note that due to the small gap in the middle of the 3-loop "8", the radius of the two circles forming the "8" configuration is slightly larger than the idealized radius $L/2\pi$ shown in Fig. 1 in the main text, and thus its dimensionless initial curvature, $L\kappa_0/2\pi$, is slightly smaller than 1. Here, we use the transition state of the 3-loop line obtained by bending three layers together, i.e., the 3-loop "8" without edge contact in the middle, as the initial configuration, whose curved edges have a dimensionless initial curvature $L\kappa_0/2\pi$ = 0.98. From Fig. S6, it is found that when the dimensionless natural curvature, $L\kappa_n/2\pi$, is within the range (0.64, 1.12), the 3-loop "8" inverts into the 3-loop line. However, when the dimensionless natural curvature is within the range (1.13, 1.38), the 3-loop "8" folds into a 6-loop "8".

Transition behavior of the 3-loop "8" with different natural curvatures, triggered by bending three layers together at a pair of edges (referred to as edge bend in the main text), is illustrated in Fig. S7. Results demonstrate that the 3-loop "8" with dimensionless natural curvature within the range (0.64, 0.74) inverts into the 3-loop line, but within the range (0.75, 1.38) folds into the 6-loop "8". Combined with the findings in the case of corner bend, we can find that in the curvature range (0.75, 1.12), the 3-loop "8" transitions to the 3-loop line state under corner bend, while transitions to the 6-loop "8" state under edge bend. Therefore, transition behavior of the 3-loop "8" depends on the natural curvature as well as the loading positions of the external stimuli.

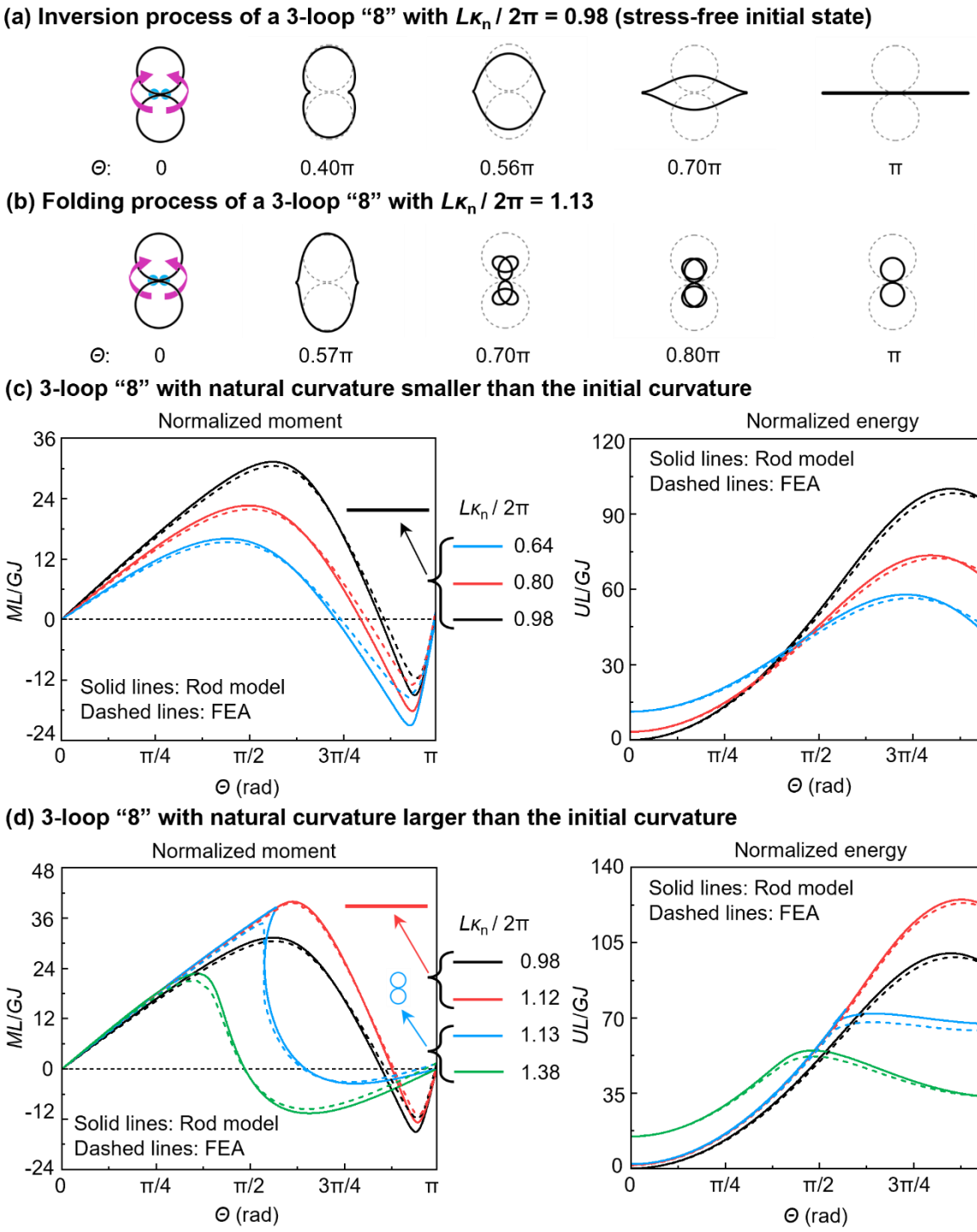

Fig. S6. Transition behavior of 3-loop "8" with different natural curvatures under corner bend. (a) Inversion process (top view) of a 3-loop "8" with a dimensionless natural curvature $L\kappa_n/2\pi = 0.98$, which has a stress-free initial state. (b) Folding process (top view) of a 3-loop "8" with a dimensionless natural curvature $L\kappa_n/2\pi = 1.13$. The blue dots denote the loading positions. (c) Normalized moment and energy versus bending angle of 3-loop "8" with natural curvatures smaller than the initial curvature. (d) Normalized moment and energy versus bending angle of 3-loop "8" with natural curvatures larger than the initial curvature. The 3-loop "8" with dimensionless natural curvature in the range (0.64, 1.12) inverts into the 3-loop line, and in the range (1.13, 1.38) folds into a 6-loop "8", as indicated by the insets.

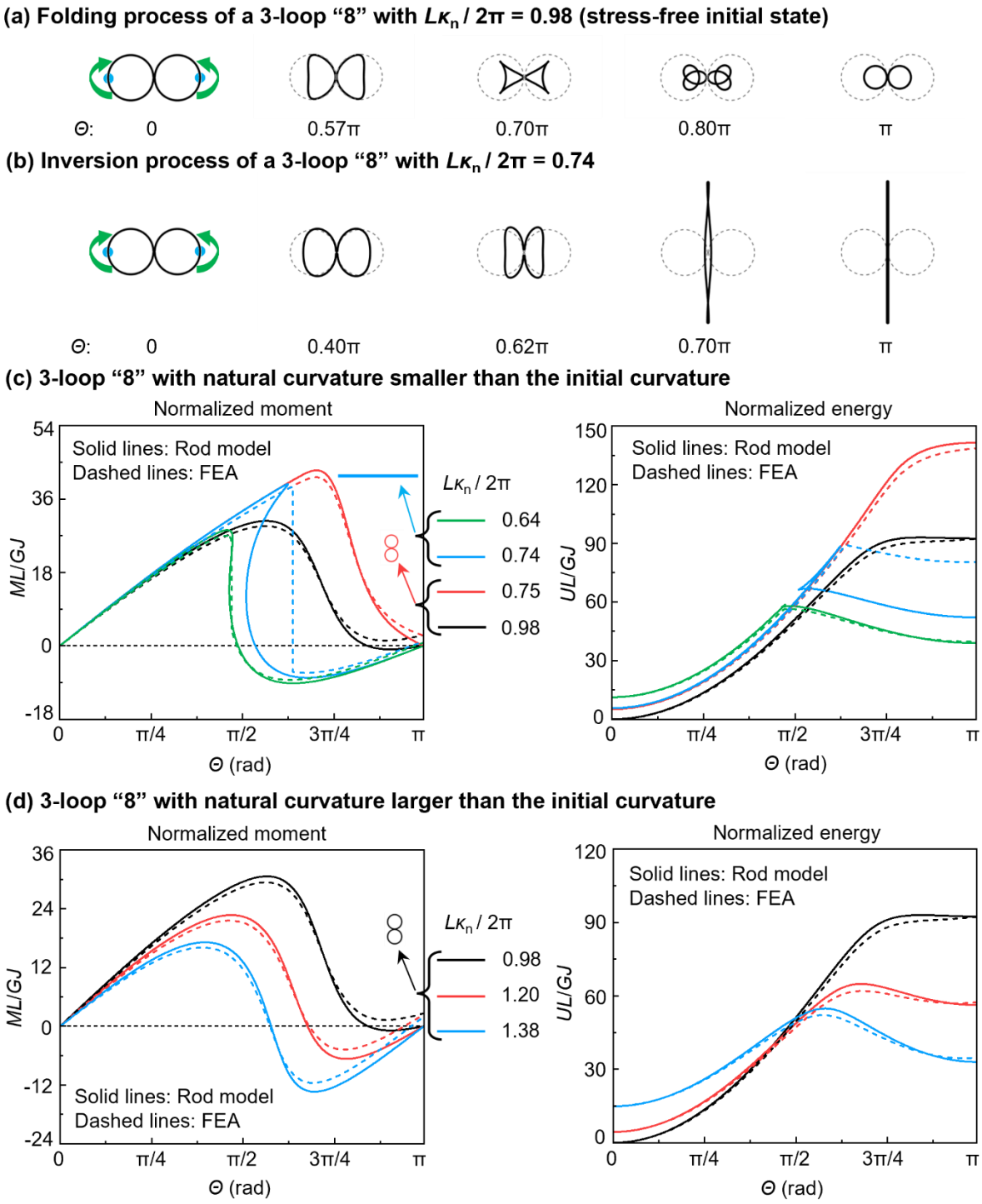

Fig. S7. Transition behavior of 3-loop "8" with different natural curvatures under edge bend. (a) Folding process (top view) of a 3-loop "8" with a dimensionless natural curvature $L\kappa_n/2\pi = 0.98$, which has a stress-free initial state. (b) Inversion process (top view) of a 3-loop "8" with a dimensionless natural curvature $L\kappa_n/2\pi = 0.74$. The blue dots denote the loading positions. (c) Normalized moment and energy versus bending angle of 3-loop "8" with natural curvatures smaller than the initial curvature. (d) Normalized moment and energy versus bending angle of 3-loop "8" with natural curvatures larger than the initial

curvature. The 3-loop "8" with dimensionless natural curvature in the range (0.64, 0.74) inverts into the 3-loop line, and in the range (0.75, 1.38) folds into a 6-loop "8", as indicated by the insets.

3.2. Bending in different layers

Transition behavior of the 3-loop line with different natural curvatures under bending at corners in different layers, predicted by FEA, is presented in Fig. S8. Compared to the case of bending three layers together in which the 3-loop line always inverts into a 3-loop "8" configuration, the 3-loop line under bending in different layers transitions either to the star hexagram state or to the 3-loop "8" state. In particular, for the 3-loop line with a zero or negative natural curvature, the edges of its transition states have no contact in the middle. For the 3-loop line with a positive natural curvature, the edges of its transition state contact in the middle. Moreover, it is shown from Figs. S8(c) and S8(d) that when the dimensionless natural curvature is smaller than −0.73 or larger than 0.73, the 3-loop line in the initial state is no longer stable, which means that the lower and upper stability limits for the dimensionless natural curvature of the 3-loop line is −0.73 and 0.73, respectively, which is in great agreement with the theoretical prediction in Part I, namely −0.75 and 0.75, for the case of h/t=4 and ν=1/3.

Fig. S9 shows the transition behavior of the 3-loop "8" with different natural curvatures under bending at corners in different layers predicted by FEA. As can be observed, the 3-loop "8" could unfold to the daisy hexagram or the 6-circle hexagram with cusps pointing outwards by bending in different layers, which is also different than the case of bending three layers together. Also, we can find from Figs. S9(c) and S9(d) that when the dimensionless natural curvature is smaller than 0.64 or larger than 1.38, the 3-loop "8" will become unstable in the initial state. In other words, the lower and upper stability limits for the dimensionless natural curvatures of the 3-loop "8" are 0.64 and 1.38, respectively, which agree well with the theoretical predictions in Part I, i.e., 0.63 and 1.41, when h/t=4 and ν=1/3.

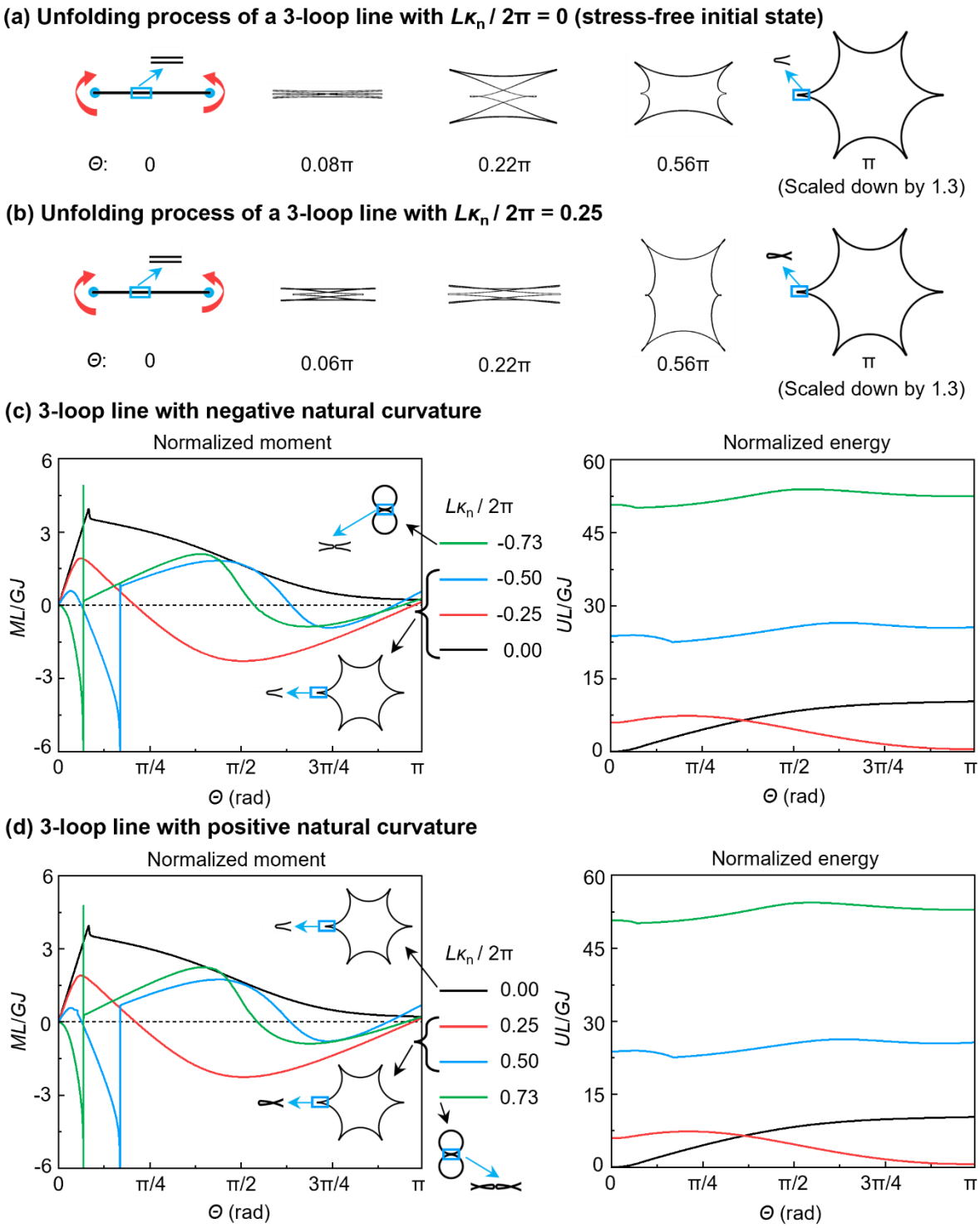

Fig. S8. Transition behavior of 3-loop lines with different natural curvatures under bending at corners in different layers predicted by FEA. (a) Unfolding process (top view) of a 3-loop line with a dimensionless natural curvature $L\kappa_n/2\pi = 0$, which has a stress-free initial state. (b) Unfolding process (top view) of a 3-loop line with a dimensionless natural curvature $L\kappa_n/2\pi = 0.25$. The blue dots denote the loading positions. (c) Normalized moment and energy versus bending angle of 3-loop lines with negative natural curvatures.

(d) Normalized moment and energy versus bending angle of 3-loop lines with positive natural curvatures. The insets represent the states to which 3-loop line transition for different natural curvatures.

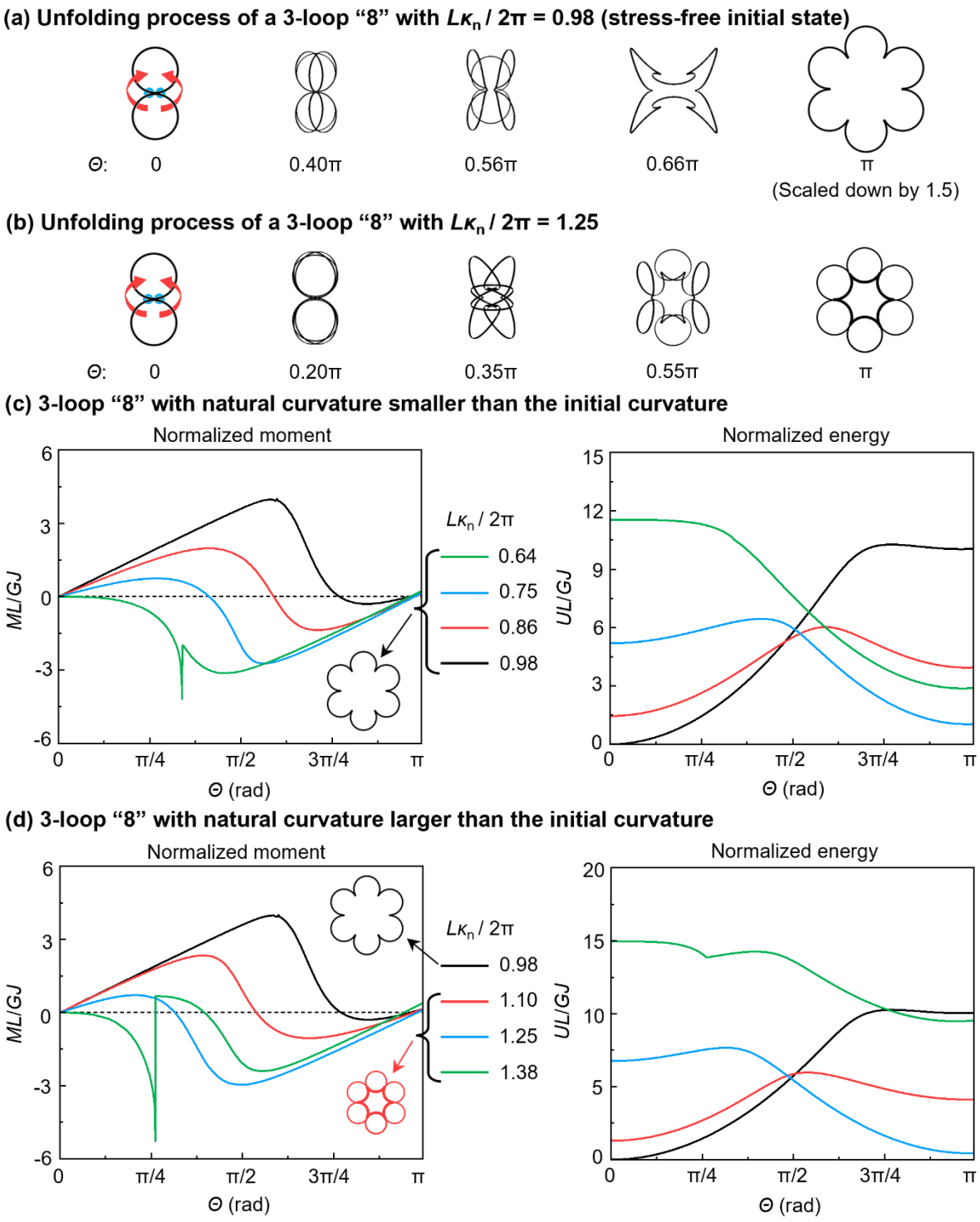

Fig. S9. Transition behavior of 3-loop "8" with different natural curvatures under bending at corners in different layers predicted by FEA. (a) Unfolding process (top view) of a 3-loop "8" with a dimensionless natural curvature $L\kappa_n/2\pi = 0.98$, which has a stress-free initial state. (b) Unfolding process (top view) of a

3-loop “8” with a dimensionless natural curvature $L\kappa_n/2\pi = 1.25$. The blue dots denote the loading positions. (c) Normalized moment and energy versus bending angle of 3-loop “8” with natural curvatures smaller than the initial curvature. (d) Normalized moment and energy versus bending angle of 3-loop “8” with natural curvatures larger than the initial curvature. The insets represent the states to which 3-loop “8” transition for different natural curvatures.